SCIENTIFIC REPORTS

OPEN

Full-surface emission of graphene-based vertical-type organic light-emitting transistors with high on/off contrast ratios and enhanced efficiencies

Received: 8 January 2019
Accepted: 9 April 2019
Published online: 19 April 2019

Byoungchoo Park, Won Seok Lee, Seo Yeong Na, Jun Nyeong Huh & In-Gon Bae

Surface-emitting organic light-emitting transistors (OLETs) could well be a core element in the next generation of active-matrix (AM) displays. We report some of the key characteristics of graphene-based vertical-type organic light-emitting transistors (Gr-VOLETs) composed of a single-layer graphene source and an emissive channel layer. It is shown that $FeCl_3$ doping of the graphene source results in a significant improvement in the device performance of Gr-VOLETs. Using the $FeCl_3$-doped graphene source, it is demonstrated that the full-surface electroluminescent emission of the Gr-VOLET can be effectively modulated by gate voltages with high luminance on/off ratios (~10^4). Current efficiencies are also observed to be much higher than those of control organic light-emitting diodes (OLEDs), even at high luminance levels exceeding 500 cd/m^2. Moreover, we propose an operating mechanism to explain the improvements in the device performance *i.e.*, the effective gate-bias-induced modulation of the hole tunnelling injection at the doped graphene source electrode. Despite its inherently simple structure, our study highlights the significant improvement in the device performance of OLETs offered by the $FeCl_3$-doped graphene source electrode.

Organic light-emitting transistors (OLETs) have been developed by integrating the ability of organic light-emitting diodes (OLEDs)[1–6] to generate light with the electrical-switching functionality of organic field-effect transistors (FETs)[7,8] into a single device structure[9–29]. In OLETs, the current flowing through emissive semiconductor channel layers can be modulated by the gate voltage, which can also change the electroluminescent (EL) emission brightness from the dark off-state to the bright on-state[9–29]. In addition to such EL switching functionality, OLETs have other advantages over OLEDs, such as relatively high luminance efficiency and external quantum efficiency[13,14]. Thus, OLETs are of key interest, as they can provide a unique type of device architecture for investigating fundamental opto-electronic properties related to the charge carrier injection, transport, and radiative exciton recombinations in organic semiconducting materials. Moreover, due to their compact architecture, they can be used to develop integrated organic opto-electronic devices such as highly efficient light sources, optical communication systems, and/or electrically driven organic lasers[11–18].

For these principal reasons, the luminance from an OLET can be modulated without any additional driving devices, and displays using OLETs thus offer the additional advantage of reducing the number of high mobility-driving thin film transistors (TFTs) and simplifying the inherent complexity of the circuits of conventional active-matrix (AM) OLEDs[14,17,20]. In this sense, OLETs can be an effective means of increasing the aperture ratio (the light-emitting area as a proportion of the total area of the device), making it higher than that (~34%) of a typical AM-OLED[17,20]. Hence, surface-emitting OLETs may offer an attractive alternative to conventional AM displays as a key element in the development of next-generation AM display technology[17,20].

Most OLETs have lateral source-drain geometries but exhibit line-, band-, or circular-type emission characteristics in a limited zone between the source and drain electrodes[9–20]. Thus, much effort has been made to improve the device performance and to extend the light emission area; multilayer structures[12,14,16] and/or modified

Department of Electrical and Biological Physics, Kwangwoon University, Wolgye-Dong, Nowon-gu, Seoul, 01897, Republic of Korea. Correspondence and requests for materials should be addressed to B.P. (email: bcpark@kw.ac.kr)

electrodes[18–20] have been suggested to control the charge injection, charge transport, and charge carrier recombinations in the emissive channel layers of these devices.

To obtain highly increased source drain current flows even at low gate voltages, vertical OLETs (VOLETs) were also constructed with short channel lengths by coupling a static induction transistor structure[21,22], constructing a metal insulator semiconductor structure[23,24], or using micro-networks with periodic vacancies in a vertical configuration[25,26]. These devices have shown stripe-type or quasi-surface emission patterns. In these cases, a reliable and high-resolution patterning method for electrodes and/or an insulating charge-restriction layer would be crucial to control the leakage currents and switching characteristics.

In another effort, a novel type of VOLET and a related fully functional display were developed using a source electrode consisting of randomly distributed carbon nanotubes (CNTs)[27–29]. The CNT-based VOLET (CNT-VOLET) has shown a number of remarkable improvements, such as highly bright and efficient full-surface emissions with high on/off ratios[27,28]. This good switching ability was mainly attributed to the gate-voltage-induced modulation of the lateral (or horizontal) Schottky barrier height for the dilute network of the CNT source electrode in the CNT-VOLET[27,28]. Nevertheless, the CNT-VOLET may experience non-uniformity as well as poor connectivity of the CNTs in the source electrode[8,25,26]. In addition, the irregular interface between the CNT source electrode and its adjacent functional layer may act as traps to hinder the charge transport[25,26]. Moreover, the CNT electrode typically forms a very rough surface, thus requiring a fairly thick adjacent functional layer[8,28]. Thus, the ultimate goal of simple and reliable OLETs capable of high device performance with good switching ability remains unmet.

In this article, we report on the first use of a VOLET with a homogeneous, smooth, and easily processable graphene layer as the source electrode, together with an emissive channel layer. As a two-dimensional material in the form of a single layer with a carbon-based hexagonal lattice structure bonded in the sp^2 configuration[30–32], graphene has been used as a transparent electrode material in small OLEDs, as a proof of concept[33–35]. Despite the low dimensionality of graphene, similar to that of CNTs[31,32], the successful operation of full-surface EL light emission from a VOLET based on graphene has not yet been reported, as the work function (~4.6 eV) of pristine graphene is too low for the hole injection[33–35]. We describe the fabrication and characterization of a simple graphene-based VOLET (Gr-VOLET) with a $FeCl_3$-doped single-layer graphene (SLG) source electrode. We find that the EL properties of the Gr-VOLET can be efficiently modulated with high luminance on/off ratios (~10^4) through the application of gate voltage. More interestingly, our Gr-VOLETs with doped SLG sources are shown to exhibit greatly improved device performance, especially for their higher current efficiencies as compared to those of control OLEDs, even at high luminance levels exceeding 500 cd/m^2, making them all the more attractive. We discuss the operating mechanism that explains these significant improvements in the device performance; *i.e.*, the effective modulation of the hole tunnelling injection from the $FeCl_3$-doped graphene source.

Results and Discussion

Operating characteristics of Gr-VOLETs. Our first challenge relates to the structure and operating characteristics of our Gr-VOLET, including the bottom indium tin oxide (ITO) gate, the Al_2O_3 gate dielectric layer, the SLG source, the functional channel layers including the organic light-emitting layer (EML) of the Super Yellow (SY) conjugated copolymer, and the Al metal drain, in sequence (Fig. 1a, see also Methods and Supplementary Fig. S1a for details of the structure and layer thicknesses). During the operation of the Gr-VOLET, the electron injection occurs from the Al drain into the channel layer, and the hole injection from the SLG source can be modulated by adjusting the gate voltage V_{GS}, as discussed below. Figure 1b shows the EL light emissions of a sample Gr-VOLET operating under different V_{GS} levels with a fixed source-drain voltage V_{SD} of 3.8 V. As shown in the figure, the EL light emission is uniformly bright (in the fully on-state), grey, and dark (off-state) over the entire surface of the active area for negative, zero, and positive V_{GS} values, respectively. (See also Supplementary Information Video 1 and Supplementary Fig. S1b for images of the device in the dark). Hence, V_{GS} essentially influences the hole injection and current flow through the emissive channel layer and thus may contribute to the charge balance for efficient hole-electron recombinations in the channel layers. The EL emission spectra observed are nearly identical to those obtained from a conventional ITO-OLED (Fig. 1c). Furthermore, the temporal responses of the Gr-VOLET with respect to step changes in V_G show rapid rising and falling times of 4.7 ms and 2.8 ms, respectively (Fig. 1d), which are also comparable to those of conventional OLEDs and much faster than those of traditional liquid crystal displays (LCDs)[5]. The above characteristics highlight several interesting features of our Gr-VOLET. To investigate its distinct characteristics further, we tested three types of SLG materials as source electrodes; (i) p-doped SLG with $FeCl_3$ (hereafter SLG_1 for fabricating Gr-$VOLET_1$), where $FeCl_3$ doping is done spontaneously during the graphene transfer process, as shown previously[35]; (ii) pristine (intrinsic) SLG, cleaned by an electrochemical process[35], as a comparative reference (SLG_2 for Gr-$VOLET_2$); and (iii) SLG coated with a conventional hole-injection layer (HIL) of (3,4-ethylenedioxythiophene):poly(styrene sulfonate) (PEDOT:PSS)[34] as a second comparative reference (SLG_3 for Gr-$VOLET_3$). The basic properties of the three SLG sources (with low porosities below 0.1%) are shown in Supplementary Fig. S2,S3 and S4 and are summarised in Table 1.

We now describe the detailed output current and luminance characteristics of the three prototype Gr-VOLETs mentioned above. For comparative purposes, we also observed the diode characteristics of the Gr-VOLETs with the gate electrodes disconnected from the external circuits (Gr-OLEDs) (Fig. 2a and Supplementary Figs S5a and S6a). As shown, the current density-voltage (J_D-V_{SD}) and luminance-voltage (L-V_{SD}) characteristics of the Gr-VOLETs present four key characteristics: (1) the J_D-V_{SD} characteristics are similar to those of a diode without current saturation, which were generally observed in vertical-type organic field-effect transistors due to the short vertical channel lengths[8], (2) similar behaviours to the J_D-V_{SD} curves were observed in the L-V_{SD} characteristics, (3) both J_D and L for a given V_{SD} increase with a decrease in the negative V_{GS}, even at a low V_{SD}, which shows that current modulation by V_{GS} can change EL emission brightness. Hence, the V_{GS}-dependent turn-on voltage

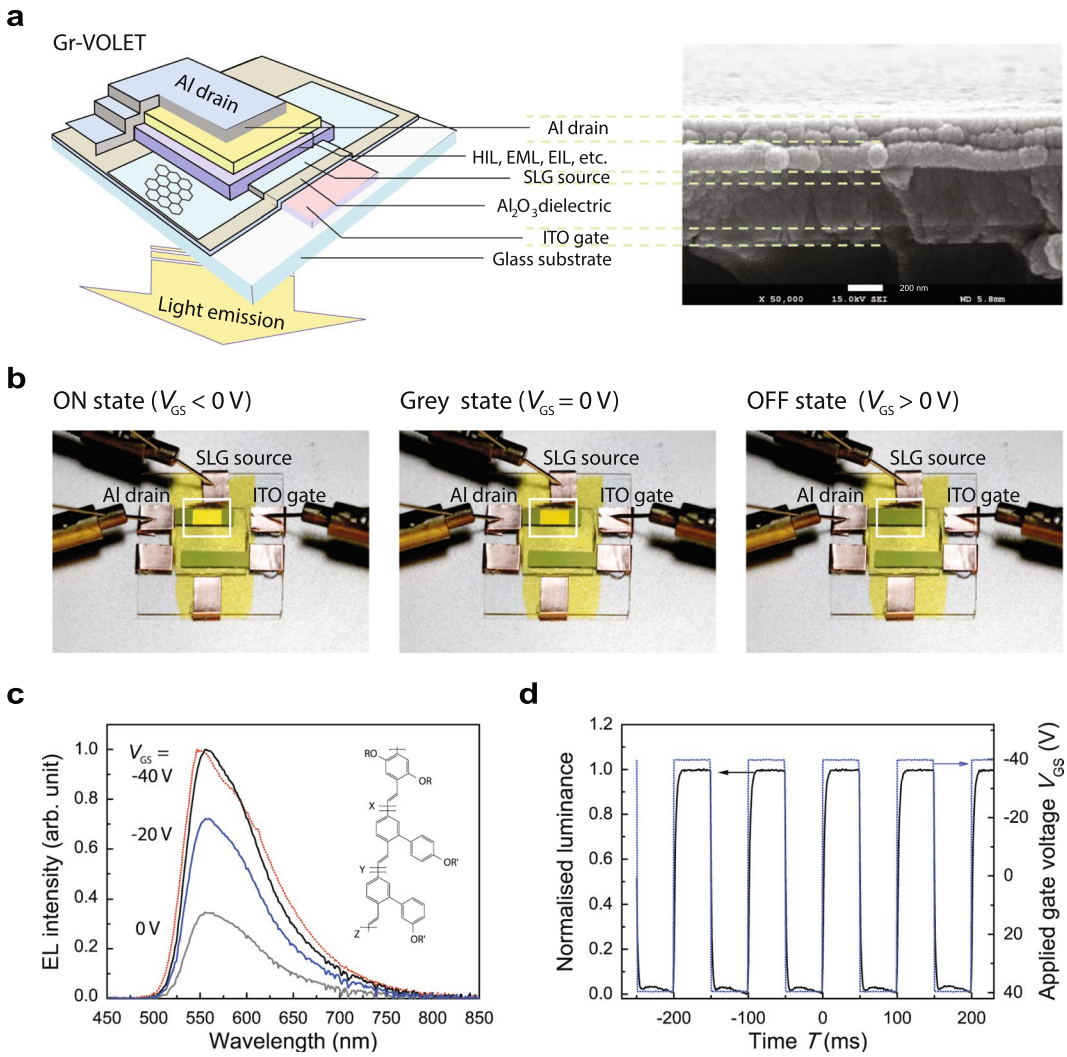

Figure 1. Structure and operation of graphene-based vertical organic light-emitting transistors (Gr-VOLETs). (**a**) Schematic illustration of the structure and a SEM image of a cross-sectional slice of the Gr-VOLET with a single-layer graphene (SLG) source, stacked layers of organic functional channel layers, an Al drain, and an ITO gate separated with an Al_2O_3 gate dielectric (scale bar: 200 nm). (**b**) Light emission from a Gr-VOLET (4 mm × 2 mm, white squares) for three different gate voltages of V_{GS} for a fixed source-drain voltage, V_{SD}, of 3.8 V (see also Supplementary Video S1 and Supplementary Fig. S1b). (**c**) Relative electroluminescent spectra of a Gr-VOLET (solid curves) and of a corresponding control ITO-OLED (dotted curve). The molecular structure of Super Yellow (SY) is shown in the inset. (**d**) Temporal response of a Gr-VOLET with respect to the step gate voltages for a fixed V_{SD} of 3.8 V.

SLGs	Sheet resistance, (kΩ/square)	Work function* (eV)	Dirac point energy* (eV)	Hole/electron mobility ($cm^2/(V\,s)$)
SLG_1	1.20	5.21 ± 0.07	4.89	410/–
SLG_2	2.40	4.70 ± 0.10	4.44	580/530
SLG_3	1.40	5.21 ± 0.06	4.98	530/–

Table 1. Summary of the basic electronic properties of the SLGs studied here. Average values were obtained from five individual devices for each of the device configurations studied.

(V_{onset}) can be reduced to well below V_{onset} of the Gr-OLED, and (4) both J_D and L also depend on the direction of the change of V_{GS}, *i.e.*, increasing (upward)/decreasing (downward), implying hysteretic behaviour. Among the Gr-VOLETs, interestingly, the Gr-VOLET device with the doped SLG_1 source ($Gr\text{-}VOLET_1$, Fig. 2a) exhibits highly improved device performance, superior to that of $Gr\text{-}OLED_1$. For example, at $V_{GS} = -40$ V, the J_D value is higher than that of $Gr\text{-}OLED_1$ and the luminance reaches $L \sim 2{,}000\ cd/m^2$ at $V_{SD} = 6.0$ V ($V_{onset} = 2.3$ V), which is more than twice that ($L \sim 740\ cd/m^2$ and $V_{onset} = 2.5$ V) of $Gr\text{-}OLED_1$. These outcomes indicate improved and

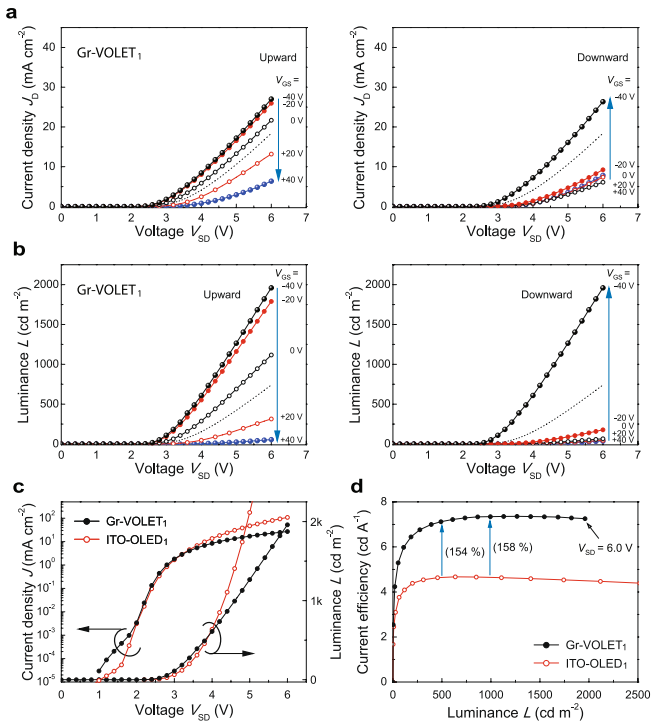

Figure 2. Output characteristics of Gr-VOLET$_1$ and comparison with the control ITO-OLED. Gate-voltage (V_{GS})-dependent current density-voltage (J_D-V_{SD}) (**a**) and luminance-voltage (L-V_{SD}) (**b**) characteristics of Gr-VOLET$_1$ with a $FeCl_3$-doped SLG$_1$ source for upward (left) and downward (right) changes in V_{GS}. For comparison, the characteristics of a gate-disconnected Gr-VOLET$_1$ (*i.e.*, Gr-OLED$_1$) are also shown (dotted curves). J-L-V (**c**) and η_C-L (**d**) comparisons of Gr-VOLET$_1$ in the bright on-state ($V_{GS} = -40$ V) with its respective ITO-based control OLED (ITO-OLED$_1$, ITO/SY/CsF/Al).

Devices	$\eta_{C\,Gr\text{-}OLET}$ (cd/A)	$\eta_{C\,OLED}$ (cd/A)	$\eta_{C\,Gr\text{-}OLET}/\eta_{C\,OLED}$[a]
Gr-VOLET$_1$	7.13	4.64	1.54
Gr-VOLET$_2$	2.92	4.64	0.63
Gr-VOLET$_3$	3.72	5.17	0.72

Table 2. Comparison of the current efficiencies of Gr-VOLETs ($\eta_{C\,Gr\text{-}OLET}$) and ITO-based control OLEDs ($\eta_{C\,OLED}$) with their $\eta_{C\,Gr\text{-}OLET}/\eta_{C\,OLED}$ ratios at a luminance level of 500 cd/m^2. [a]Ratio of the current efficiency of a full-surface emitting Gr-OLET to that of the control ITO-based OLED for a given luminance level of 500 cd/m^2.

balanced charge (hole) injections from the SLG$_1$ source in the case of a negative V_{GS}. Conversely, at $V_{GS} = +40$ V, J_D and L of Gr-VOLET$_1$ are much lower, possibly due to the switching off of the hole injection from the SLG source. The highest values observed for the peak on/off ratios of J_D and L were approximately 10^2 and 10^4, respectively, at $V_{GS} = \pm 40$ V. This gate-bias-induced modulation effect of Gr-VOLET$_1$ is shown to be more efficient than those of the other Gr-VOLETs tested here with the pristine (pure) SLG$_2$ source (Gr-VOLET$_2$), or even with the PEDOT:PSS HIL-coated SLG$_3$ source (Gr-VOLET$_3$).

We then estimated the device performance capabilities of the Gr-VOLETs in the on-state ($V_{GS} = -40$ V), comparing these with control OLEDs fabricated using the same batch process on ITO anodes (ITO-OLEDs) (Fig. 2b and Supplementary Figs S5b and S6b). As shown, only Gr-VOLET$_1$ exhibits luminance higher than that of the control ITO-OLED (ITO/SY/CsF/Al) in the source-drain voltage region $V_{SD} < 4.0$ V (Fig. 2b). For example, when $V_{SD} = 3.8$ V, Gr-VOLET$_1$ emitted luminance of 490 cd/m^2, while the control ITO-OLED emitted luminance of 455 cd/m^2 at $V = 3.8$ V. Moreover, Gr-VOLET$_1$ was found to be more efficient than the control ITO-OLED, in contrast to the other Gr-VOLETs (Fig. 2c and Supplementary Figs S5c and S6c). For instance, at a luminance level of 500 cd/m^2, Gr-VOLET$_1$ emitted EL light with current efficiency η_C of 7.13 cd/A, which is approximately 1.54 times higher than that (4.64 cd/A) of the control ITO-OLED ($\eta_{C\,Gr\text{-}OLET}/\eta_{C\,OLED} = 1.54$). Even at luminance levels exceeding 2,000 cd/m^2, Gr-VOLET$_1$ maintains an enhanced $\eta_{C\,Gr\text{-}OLET}/\eta_{C\,OLED}$ ratio of ~1.62. It is therefore clear that Gr-VOLET$_1$ has highly enhanced current efficiency compared to other devices investigated (Table 2). This offers another important advantage: given this level of enhanced current efficiency, the brightness of the device can be maintained with a lower J_D, promising a longer device lifetime[6]. It is noteworthy that η_C (7.13 cd/A) for Gr-VOLET$_1$ was approximately 1.38 times higher than that (5.17 cd/A) of ITO-OLED$_3$, the latter possessing the

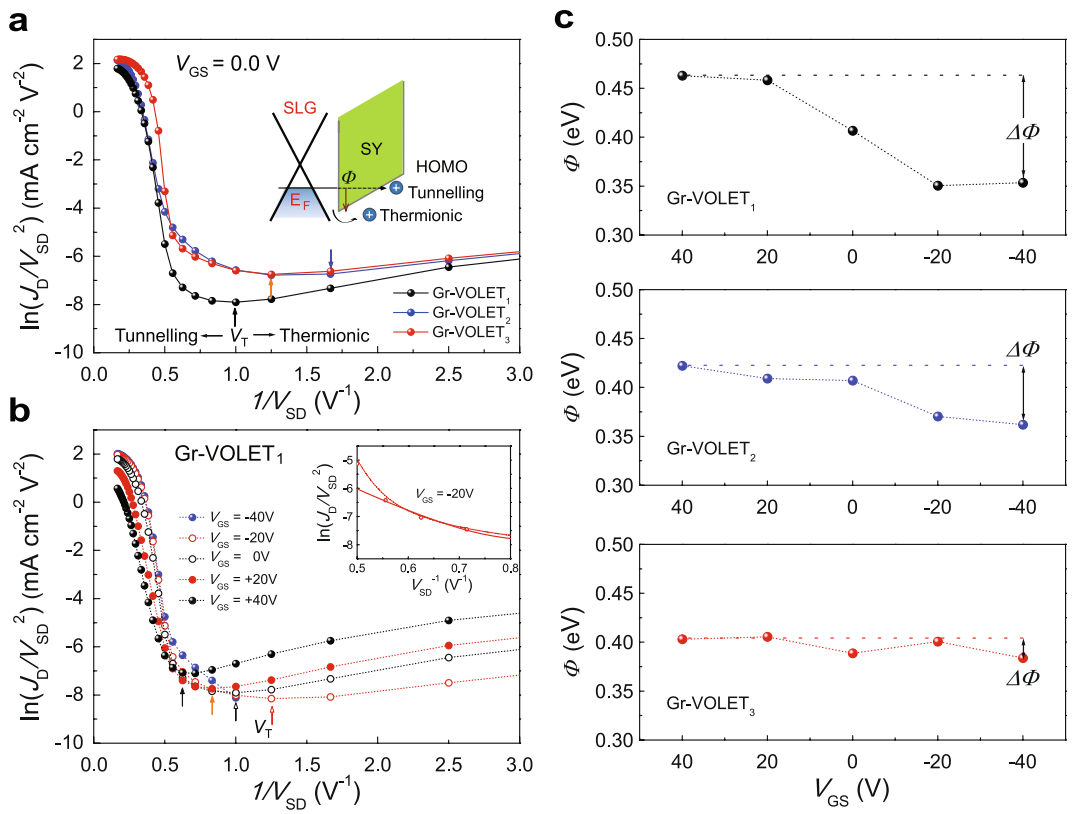

Figure 3. Charge injection processes in Gr-VOLETs. Fowler-Nordheim plot, $\ln(J_D/V_{SD}^2)$ vs $1/V_{SD}$, for Gr-VOLETs with different SLG sources at $V_{GS} = 0$ V (**a**) and with the SLG_1 source at various V_{GS} levels (**b**) for upward V_{GS} changes. The inset in (**a**) shows a schematic energy band diagram of the thermionic emission and tunnelling at the SLG/SY interface along the normal direction of the interface between the SLG and the SY channel layer. The inset in (**b**) shows an example of the theoretical fittings based on the tunnelling current model (solid curve). (**c**) Gate-bias-modulated hole tunnelling barrier height, Φ, extracted from the fittings in the hole-dominant regimes. $\Delta\Phi$: gate-bias-induced Φ modulation when $V_{GS} = \pm 40$ V.

optimised HIL of PEDOT:PSS (Supplementary Fig. S6c). Thus, it is clear that the SLG_1 source in Gr-$VOLET_1$ provides amplification of both the emission and current efficiency, although further optimization of the drain electrodes is still possible.

Charge injection process at SLG sources. Our investigation also focused on the hole injection mechanism from the SLG source into the SY channel layer. To be injected across the SLG/SY interface, the holes must overcome the potential barrier at the interface either via thermionic emission or tunnelling processes[36–41]. Figure 3a shows examples of Fowler-Nordheim (F-N) plots[36–41], $\ln(J_D/V_{SD}^2)$ vs $1/V_{SD}$, for the three Gr-VOLETs when $V_{GS} = 0$ V during upward changes in V_{GS}. All of the plots show two distinct hole injection processes with the transition voltage (V_T), at which value the injection mechanism changes from Schottky thermionic emission to tunnelling[39–41].

Figure 3b presents F-N plots of a typical Gr-$VOLET_1$ at various values of V_{GS} during upward V_{GS} changes. It is interesting to note that V_{GS} affects both Schottky thermionic emission and tunnelling; thus, V_T strongly depends on V_{GS}. It is also noteworthy that because the EL emission from the Gr-VOLETs occurs when $V_{SD} > V_{onset}$, higher than V_T, the main hole injection process for light emission is tunnelling injection in the Gr-VOLETs. According to a modified tunnelling current model[42], the tunnelling current density (J) for a single charge carrier through a triangular barrier at a metal/polymer junction is related to the potential barrier height Φ and the temperature T: $\ln(J/V^2) = -P_1/V + \ln(P_2/V) - \ln[\sin(P_3/V)]$, with $\Phi = (3/2)\,\pi k_B T\,(P_1/P_3)$, where k_B is the Boltzmann constant, and P_i denotes parameters related to Φ[42]. This relationship allows the F-N curves to be analysed, and the potential barrier heights Φ at the SLG/SY interfaces between the Fermi level of the SLGs and the highest occupied molecular orbital (HOMO) level (~5.3 eV) of the SY channel layer[35] to be obtained (Fig. 3c), all of which are in reasonable agreement with values in the literature[43]. Among the SLG/SY interfaces, the SLG_1/SY interface exhibited the strongest gate-bias-induced Φ modulation ($\Delta\Phi$) along the direction normal to the interface; *i.e.*, $\Delta\Phi$ at $V_G = \pm 40$ V was approximately 110 meV, which is much higher than the values of $\Delta\Phi$ for SLG_2/SY (~60 meV) and SLG_3/SY (~20 meV). This strongest gate-bias-induced Φ modulation of the $FeCl_3$-doped SLG_1 source leads to the efficient modulation of the device performance of Gr-$VOLET_1$ as tested here. Note that when $V_{SD} > V_{onset}$, the theoretical predictions begin to deviate from the experimental data, mainly due to minority carrier (electron) injections into the SY channel layer from the Al drain. Nevertheless, tunnelling at the SLG/SY interface is the major

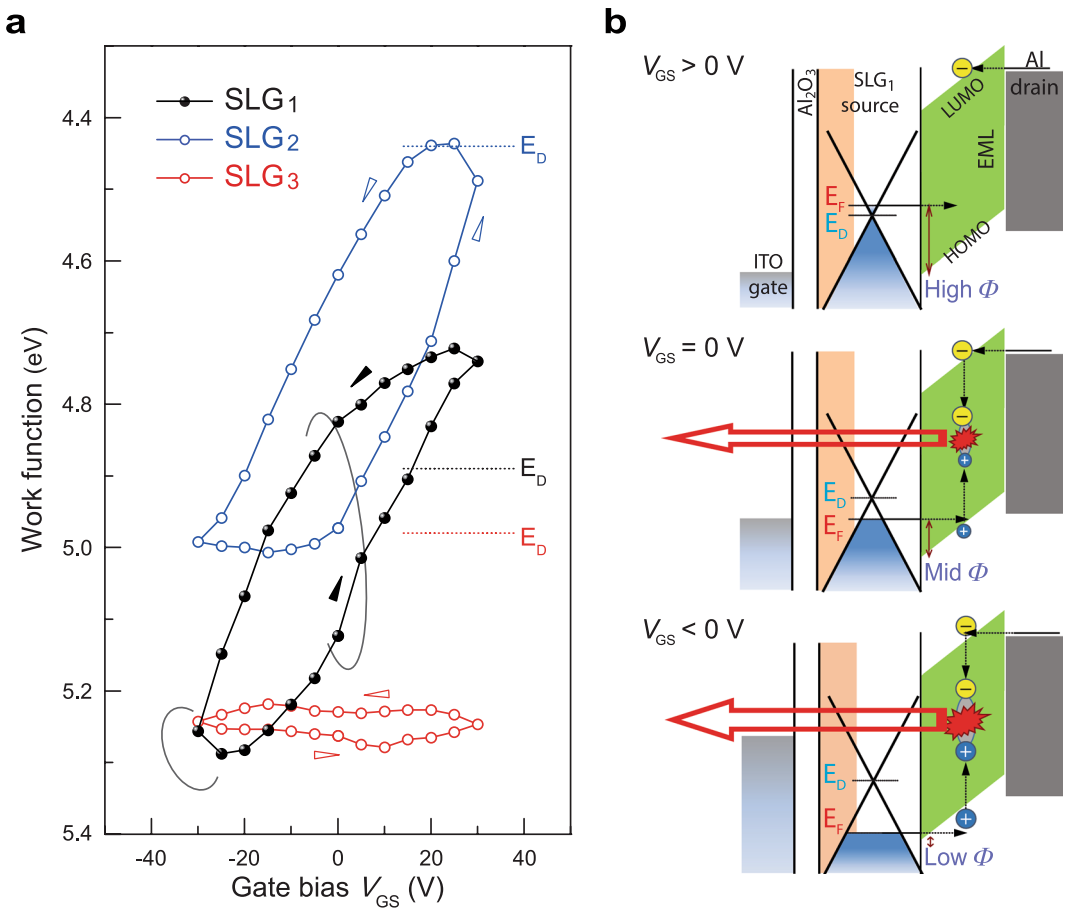

Figure 4. Gate-bias-induced modulation of SLG work functions and operation mechanism of Gr-VOLETs. (**a**) Gate-bias-induced modulation of the work functions of SLG sources on the VOLET substrates. (**b**) Energy-level diagrams of Gr-VOLET$_1$ for high, mid, and low Φs at three distinct values of V_{GS} at a given V_{SD}. Φ depicts the tunnelling barrier height for the hole injection. E_D: Dirac point energy of the SLG source used.

hole injection process, being responsible for the radiative recombination of electron-hole pairs. This analysis is also supported by an inspection of the weak dependence on T of J_D-V_{SD} and V_T for Gr-VOLET$_1$ (Supplementary Fig. S7); the other injection process, Schottky thermionic injection, is in contrast strongly dependent on T[36,39,40]. Therefore, the tunnelling analysis provides clear evidence that our device operates via the modulation of the vertical barrier height along the direction normal to the source surface (*i.e.*, parallel to the gate field direction), in contrast to the CNT-VOLET based on lateral (or horizontal) Schottky barrier height modulation along the horizontal direction on the source surface (*i.e.*, perpendicular to the gate field direction)[27,28], and different as well from conventional graphene-based barristors that operate via the modulation of the Schottky thermionic injection[44]. It is also noted that if one considers the further contribution of the gate field to the electric field inside the channel layer together with an appropriate dielectric constant of the channel layer, one may then obtain a more precise value of the barrier height from the F-N analysis for the injection characteristics. However, this is beyond the scope of this report, and further details about such an analysis and a related discussion will therefore be reported elsewhere.

To gain a better understanding of the hole injection mechanism at the SLG sources, we also investigated the dependence of the Fermi levels (work functions) of the SLG sources on the gate bias using the KPFM method (see also Supplementary Fig. S3). We observe that a V_G sweep clearly modulates the work functions of the SLGs. As shown in Fig. 4a, for the pristine SLG (SLG$_2$), a large change in the work function can be observed, from 4.44 eV to 5.00 eV, by sweeping V_{GS}. However, for the doped SLG (SLG$_1$), a largely downwardly shifted modulation of the work function was observed, from 4.72 eV to 5.29 eV. This work function of SLG$_1$ is closer to the HOMO level of the SY channel layer than that of SLG$_2$ at a negative gate bias. In contrast, the PEDOT:PSS-coated SLG (SLG$_3$) shows only a minor modulation of the work function. This may be due to the negatively charged PSS in the PEDOT:PSS HIL on the SLG$_3$ source[45], which can generate a strong electrostatic field and accordingly weaken the gate-field effect, as also shown in Supplementary Fig. S6a. In addition, considerable hysteretic behaviour is apparent in all of the plots, possibly due to charge trapping in the Al_2O_3 dielectric layer[46]. These hysteretic work functions of SLGs are major causes of the hysteresis of the output characteristics of the Gr-VOLETs for upward and downward V_{GS} changes.

The above observations reveal the working principle of Gr-VOLET$_1$, as illustrated in the energy-level diagrams in Fig. 4b. At a given V_{SD}, a positive gate bias induces an upward shift of the Fermi level of the SLG$_1$ source in a

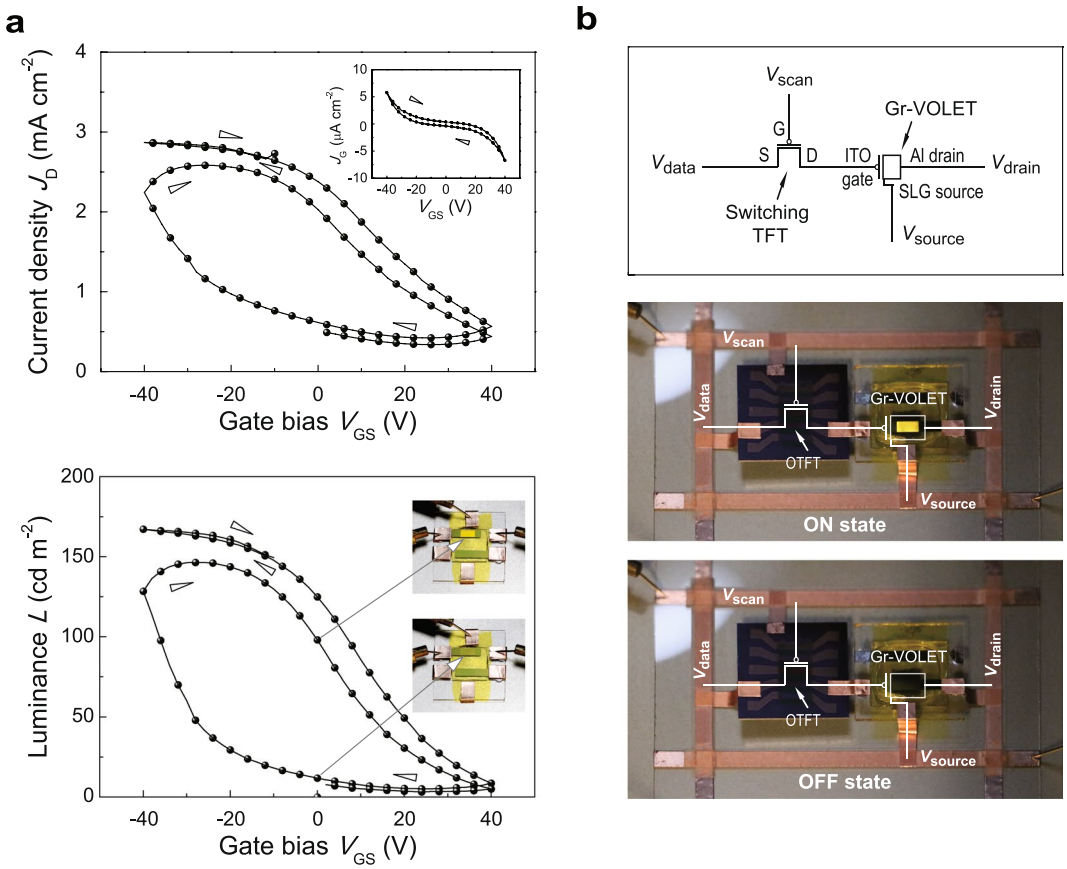

Figure 5. Transfer characteristics and Gr-VOLET switched by an OTFT. (**a**) Transfer J_D-V_{GS} (upper) and L-V_{GS} (lower) curves of Gr-VOLET$_1$ at a given V_{SD} of 3.2 V. The insets in the upper and lower panels respectively show the J_G-V_{GS} characteristics of Gr-VOLET$_1$ and two photographs of the Gr-VOLET at $V_{GS} = 0$ V for a given V_{SD}, revealing bistable-like operation. (**b**) A simple AM-OLET pixel circuit diagram of a Gr-VOLET combined with a switching TFT (upper), and two photographs of Gr-VOLET$_1$ switched by an OTFT, showing the bright on-state (middle) and the dark off-state (lower).

direction that increases the barrier height Φ, resulting in reduced tunnelling and fewer hole injections into the HOMO level of the SY channel layer. In contrast, a negative gate bias induces a downward shift of the Fermi level of the SLG$_1$ source, decreasing Φ significantly (enhancing tunnelling) and hence allowing increased hole injection and improved EL performance. Thus, together with the band-bending effect[27], the main operating mechanism of Gr-VOLET$_1$ is energy band matching, and the charge balance is thus achieved even without any HIL through gate-bias-induced modulation of the hole tunnelling injection at the SLG source, as controlled by p-type doping with $FeCl_3$. Although the work function of SLG$_3$ including the PEDOT:PSS HIL is nearly identical to that of SLG$_1$, the modulation performance of Gr-VOLET$_3$ is considerably lower than that of Gr-VOLET$_1$. This may arise when the PEDOT:PSS HIL impedes the effect of V_G on the modulation of the barrier height Φ due to its strong electrostatic field, in conjunction with the gate field-screening effect in the highly conductive PEDOT:PSS layer. Note that the changes in the potential barrier height Φ induced by V_{GS} are somewhat lower than the changes in the work functions of the SLGs caused by V_{GS}, which may be due to the field effect of V_{SD} applied to the SLG sources together with the electrostatic interaction effect via the charge transfer[47] at the SLG/SY interface (further details will be reported elsewhere).

Transfer characteristics and TFT-switching Gr-VOLETs. We now turn our attention to the transfer characteristics of Gr-VOLET$_1$. As shown in Fig. 5a, at a given V_{SD} (3.2 V), J_D increases when V_{GS} is biased towards higher negative values, and thus Gr-VOLET$_1$ is normally in the "on-state," while it is "switched off" at a positive gate bias. During the switching operation, the device exhibits a fairly low gate leakage current density (J_G) (inset in the upper panel). Similar to the output curves, no region of saturation is observed in the transfer curves for the V_G range applied. In addition, notable instances of hysteresis are clearly observed in the transfer curves, caused by the hysteretic loop of the work function of the SLG$_1$ source, as shown above; bistable-like switching operations (or memory-like effects) of Gr-VOLET$_1$ are thus verified at $V_{GS} = 0$ V, as shown in the insets in the lower panel. This property of a Gr-VOLET may allow novel applications for inexpensive and simple driving schemes with low power consumption. However, this effect may become more significant when realising high-quality grayscale; moreover, it should be carefully controlled when preparing the dielectric layer. It is also noted, as shown in the figure, that the on/off ratios of the current and luminance modulations are somewhat reduced, mainly due to the

increased leakage current between the source and drain via the deterioration of the device during the measurement process. Thus, to maintain the high on/off ratios of the devices, one should control the degradation and leakage current flows precisely.

To investigate its switching capability, we now describe an application of our Gr-VOLET combined with only one switching device, excluding any other high mobility-driving TFTs or storage capacitors as commonly used in conventional AM-OLEDs (Fig. 5b)[4]. Here, the switching device used was an organic TFT (OTFT), produced using 6,13-bis(triisopropylsilylethynyl)pentacene blended with a polymer binder of poly(a-methylstyrene), with mobility of approximately 0.1 $cm^2/(V\,s)$ (see Supplementary Fig. S8). For its operation, a V_{DS} value of ± 80 V and a V_{GS} value of -50 V were applied to the OTFT, resulting in V_{GS} applied to the gate of the Gr-VOLET being as high as ± 20 V with a fixed V_{SD} of 3.2 V for the Gr-VOLET. Most interestingly, the EL light output of the Gr-VOLET$_1$ was successfully switched from the bright on-state (middle panel) to the dark off-state (lower panel) by the OTFT operation, despite the fact that the mobility of the OTFT is much lower than that (0.6–1 $cm^2/(V\,s)$) of a typical Si TFT[4]. From this application, we contend that our Gr-VOLET shows considerable promise for reliable and high-performance AM displays.

The foregoing results clearly demonstrate the remarkable device performance of the Gr-VOLET with a $FeCl_3$-doped SLG source electrode, showing considerable promise with regard to the development of high-performance OLETs. To the best of our knowledge, this is the first demonstration of high-performance VOLETs fabricated with single-layer graphene source electrodes modified by $FeCl_3$ doping, exhibiting high on/off contrast ratios and enhanced efficiency levels.

Finally, two points should be discussed with regard to our Gr-VOLET, the first of which relates to the improvement in its performance and lifetime. The light-emitting performance and lifetime can be improved further through the additional optimization of the materials used[48]. Specifically, in place of SY used as the light-emitting material, it would be possible to use other new materials[3], including red, green, and blue light-emitting fluorescent or phosphorescent materials, which exhibit much higher brightness levels, efficiencies, and lifetimes than those of the Gr-VOLETs studied here. This could yield very bright and efficient Gr-VOLETs with long lifetimes. Second, it is possible to use a thin dielectric layer grown by other deposition methods, such as atomic layer deposition[49], rather than the thick Al_2O_3 dielectric layer used here. This could yield efficient Gr-VOLETs operating at a low V_{GS} levels, *i.e.*, below 5 V, enabling the adoption of a-Si TFT backplanes.

The advances afforded by the Gr-VOLET with its reliable switching performance, shown here even at high luminance levels, clearly demonstrate its effective light-emitting transistor functionality and make it a viable candidate for use in new voltage-driving light-emitting devices and highly integrated organic opto-electronics. Further, the combination of these Gr-VOLETs with TFT backplanes will certainly presage the development of inexpensive, fast, large-area, and high-performance AM display devices.

Conclusions

In summary, we have herein explored the characteristics of a graphene-based VOLET consisting of a homogeneous SLG source, an emissive channel layer, and an Al drain, allowing efficient switching of the device performance with variations of the gate voltage. We have verified that low-drain-voltage operations and increased brightness levels with a high luminance on/off ratio of $\sim 10^4$ can be achieved even without a HIL using a p-doped SLG source with $FeCl_3$. Moreover, the current efficiency of the Gr-VOLET was at least 1.5 times higher than that of a control ITO-based OLED at a given luminance level. These significant device performance improvements can be attributed to the efficient modulation of the hole tunnelling injection via gate-bias-induced Fermi-level control of the $FeCl_3$-doped SLG source. Together with its simple structure and easy processability, this surface-emissive device using doped graphene provides a new platform for the development of advanced light-emitting devices and/or next-generation emissive display devices.

Methods

Preparation of substrates. The transparent VOLET substrate was prepared with a pre-patterned back gate electrode consisting of 80-nm-thick ITO (30 ohm/square sheet resistance) on a glass substrate, with a sputter-deposited aluminium oxide (Al_2O_3, 400 nm) top layer as a gate dielectric layer over the ITO gate electrode (glass/ITO/Al_2O_3). The VOLET substrate used was pre-cleaned with alcohol, followed by a UV treatment for 5 min immediately prior to the fabrication of the graphene-based devices.

The lateral FET substrate was prepared using a VOLET substrate or a 300-nm-thick layer of thermally grown SiO_2 as the gate dielectric on a heavily doped n-type (100) Si wafer substrate (0.05 ohm cm) for the OTFT, together with laterally patterned metal source and drain electrodes of a 5.5-nm-thick Cr layer and a 50-nm-thick Au layer formed on the substrate via a conventional vacuum deposition process with a shield mask. The channel length (L) and width (W) of the FET were 50 μm and 1600 μm, respectively (see Supplementary Fig. S4).

Transfer of graphene. The procedure used for transferring the chemical-vapour-deposition (CVD)-grown graphene onto a target substrate[35,50], in this case a VOLET substrate, a FET substrate, or a glass substrate, is described below. The first step involves CVD growth of monolayer graphene on a copper (Cu) foil[35,50]. A clean copper foil was placed in a quartz tube chamber and the temperature was increased to 1000 °C under Ar (10 sccm). For the growth of graphene, a gas mixture of CH_4 (30 sccm) and H_2 (10 sccm) was used at $\sim 2.7 \times 10^{-2}$ Pa. The second step involved spin-coating a poly(methyl methacrylate) (PMMA) solution (950PMMAC4, MicroChem) onto the CVD-grown graphene on the copper foil at 3000 rpm for 60 s. The graphene film grown on the back side of the copper foil was then removed by atmospheric-pressure oxygen plasma. Subsequently, a PMMA-coated Cu/Gr (Cu/Gr/PMMA) block with a width of 4 mm and length of 20 mm was floated on an aqueous $FeCl_3$ solution (UN2582, Transene Co. Inc.) used to etch the copper foil entirely at 50 °C for 10 min. Subsequently, floating of the PMMA-coated Gr (Gr/PMMA) block on the $FeCl_3$ solution was maintained for a further 10 min to dope the

Gr film with $FeCl_3$, as described previously[35]. Next, the Gr/PMMA block was rinsed with deionised (DI) water several times (10 min) and transferred onto the target substrate, after which the SLG-transferred substrate was dried under reduced pressure (~1 Pa) for 1 h and left in air for one day. The PMMA supporting layer was then removed by dissolving the PMMA in chloroform (60 min), monochlorobenzene (30 min) and chloroform again (30 min) in sequence.

Cleaning and de-doping of SLGs. For cleaning and de-doping of the SLGs on the substrate, a bubble-free electrochemical (EC) treatment was carried out in a non-aqueous electrolyte of acetonitrile (ACN, 99.8%, Aldrich) with 100 mM of tetrabutylammonium hexafluorophosphate ($TBAPF_6$, >99.0%, Aldrich) using a potentiostat (DY2113, Digi-Ivy, Inc.)[35]. The SLG transferred onto the substrate was used as a working electrode with a platinum wire as a counter electrode and an Ag/AgCl electrode (3.5 M KCl) as a reference electrode[35].

The EC-cleaning treatment was conducted using freshly prepared SLG under negative voltage ranges (0.0 ~ $-0.7\,V/V_{Ag/AgCl}$) at a voltage-sweeping rate of 0.5 V/s for 10 min. After the cleaning process, the treated SLG was rinsed several times using pure ACN and DI water and then dried with N_2 gas to remove the electrolyte entirely from the SLG surface. To calibrate the electrode potentials, ferrocene (98%, Sigma Aldrich) was used as a redox probe.

Fabrication of VOLETs. The fabrication steps of the Gr-VOLET used in this study are described below (see Supplementary Fig. S1a). To construct the Gr-VOLET, SLG with an area of 4 mm by 20 mm was transferred onto the VOLET substrate, as mentioned above. The SLG electrodes used were $FeCl_3$-doped SLG (SLG_1) or EC-cleaned (pristine) SLG (SLG_2). Next, organic semiconducting materials were deposited over the source electrode regions; a 70-nm-thick channel layer of SY (poly (para-phenylene vinylene) copolymer, Merck OLED Materials GmbH) was deposited as an emissive channel layer by spin coating. Where necessary, a 20-nm-thick layer of PEDOT:PSS (CLEVIOS™ 4083, H. C. Starck Inc.) was also deposited as a HIL over the EC-cleaned SLG source by spin coating (SLG_3) prior to the deposition of the SY layer. Subsequently, a 2-nm-thick electron injection layer (EIL) of CsF and a drain electrode of Al (80 nm thick) were deposited on the top of the SY layer in sequence via thermal deposition at a rate of 0.05 nm/s under a base pressure of less than 2.7×10^{-4} Pa. The fabricated device was finally encapsulated with an epoxy resin and a glass coverslip in a nitrogen-filled glove box.

Characterisations of the SLGs and SLG-based devices. The variations in the surface roughness and surface potential of the SLG on the substrate were monitored using non-contact AFM and simultaneous KPFM (FlexAFM, Nanosurf AG), respectively, by applying an AC voltage of 1 V at a frequency of 18 kHz to a Pt/Ir-coated silicon tip. To calibrate the work function of the SLG studied here, highly oriented pyrolytic graphite (HOPG, ZYB, Optigraph GmbH) was used as a reference surface. The microscopic morphology of the device was observed by field emission scanning electron microscopy (SEM, Model JSM-6700F, JEOL Co.).

The device performance of the Gr-VOLET was measured using a chroma meter (CS-2000, Konica Minolta) in conjunction with two source meters (2636 A, Keithley). The emission characteristics of the devices were also investigated using an LED measurement system (LCS-100, SphereOptics Inc.) with an integrating sphere. For the operation of the Gr-VOLETs, source-drain voltage V_{SD} ($= -V_{DS}$) on the Al drain and gate voltage, V_{GS}, were applied with respect to the SLG source electrode, held at ground potential.

References

1. Tang, C. W. & VanSlyke, S. A. Organic electroluminescent diodes. *Appl. Phys. Lett.* **51**, 913–915 (1987).
2. Burroughes, J. H. *et al.* Light-emitting diodes based on conjugated polymers. *Nature* **347**, 539–541 (1990).
3. Takatoshi, T. *OLED display fundamentals and applications*. (John Wiley & Sons 2017).
4. Gu, G. & Forrest, S. R. Design of flat-panel displays based on organic light-emitting devices. *IEEE J. Sel. Top. Quantum Electron.* **4**, 83–99 (1998).
5. Cooper, E. A., Jiang, H., Vildavski, V., Farrell, J. E. & Norcia, A. M. Assessment of OLED displays for vision research. *J. Vis.* **13**, 1–13 (2013).
6. Tsujioka, T., Fujii, H., Hamada, Y. & Takahashi, H. Driving duty ratio dependence of lifetime of tris(8-hydroxy-quinolinate) aluminum-based organic light-emitting diodes. *Jpn. J. Appl. Phys.* **40**, 2523–2526 (2001).
7. Guo, Y. L., Yu, G. & Liu, Y. Q. Functional organic field-effect transistors. *Adv. Mater.* **22**, 4427–4447 (2010).
8. Lüssem, B., Günther, A., Fischer, A., Kasemann, D. & Leo, K. Vertical organic transistors. *J. Phys.: Condens. Matter.* **27**, 443003 (2015).
9. Muccini, M. A bright future for organic field-effect transistors. *Nat. Mater.* **5**, 605–613 (2006).
10. Cicoira, F. & Santato, C. Organic light emitting field effect transistors: advances and perspectives. *Adv. Funct. Mater.* **17**, 3421–3434 (2007).
11. Muccini, M., Koopman, W. & Toffanin, S. The photonic perspective of organic light-emitting transistors. *Laser Photonics Rev.* **6**, 258–275 (2012).
12. Capelli, R. *et al.* Organic light-emitting transistors with an efficiency that outperforms the equivalent light-emitting diodes. *Nat. Mater.* **9**, 496–503 (2010).
13. Gwinner, M. C. *et al.* Highly efficient single-layer polymer ambipolar light-emitting field-effect transistors. *Adv. Mater.* **24**, 2728–2734 (2012).
14. Ullah, M. *et al.* Simultaneous enhancement of brightness, efficiency, and switching in RGB organic light emitting transistors. *Adv. Mater.* **25**, 6213–6218 (2013).
15. Hepp, A. *et al.* Light-emitting field-effect transistor based on a tetracene thin film. *Phys. Rev. Lett.* **91**, 157406 (2003).
16. Zaumseil, J., Friend, R. H. & Sirringhaus, H. Spatial control of the recombination zone in an ambipolar light-emitting organic transistor. *Nat. Mater.* **5**, 69–74 (2006).
17. Muccini, M. & Toffanin, S. *Organic light-emitting transistors: towards the next generation display technology*. (A Wiley-Science Wise Co-Publication, 2016).
18. Hsu, B. B. Y. *et al.* Control of efficiency, brightness, and recombination zone in light-emitting field effect transistors. *Adv. Mater.* **24**, 1171–1175 (2012).

19. Yamane, K., Yanagi, H., Sawamoto, A. & Hotta, S. Ambipolar organic light emitting field effect transistors with modified asymmetric electrodes. *Appl. Phys. Lett.* **90**, 162108 (2007).
20. Muhieddine, K., Ullah, M., Maasoumi, F., Burn, P. L. & Namdas, E. B. Hybrid Area-Emitting Transistors: Solution Processable and with High Aperture Ratios. *Adv. Mater.* **27**, 6677–6682 (2015).
21. Kudo, K., Tanaka, S., Iizuka, M. & Nakamura, M. Fabrication and device characterization of organic light emitting transistors. *Thin Solid Films* **438**, 330–333 (2003).
22. Xu, Z., Li, S.-H., Ma, L., Li, G. & Yang, Y. Vertical organic light emitting transistor. *Appl. Phys. Lett.* **91**, 092911 (2007).
23. Nakamura, K. *et al*. Metal-insulator-semiconductor-type organic light-emitting transistor on plastic substrate. *Appl. Phys. Lett.* **89**, 103525 (2006).
24. Nakamura, K. *et al*. Improvement of metal-insulator-semiconductor-type organic light-emitting transistors. *Jpn. J. Appl. Phys.* **47**, 1889–1893 (2008).
25. Keum, C. M. *et al*. Quasi-surface emission in vertical organic light-emitting transistors with network electrode. *Opt. Express* **22**, 14750–14756 (2014).
26. Lee, G. *et al*. Vertical organic light-emitting transistor showing a high current on/off ratio through dielectric encapsulation for the effective charge pathway. *J. Appl. Phys.* **121**, 024502 (2017).
27. Liu, B. *et al*. Carbon-Nanotube-Enabled Vertical Field Effect and Light-Emitting Transistors. *Adv. Mater.* **20**, 3605–3609 (2008).
28. McCarthy, M. A. *et al*. Low-Voltage, Low-Power, Organic Light-Emitting Transistors for Active Matrix Displays. *Science* **332**, 570–573 (2011).
29. McCarthy, M. A. *et al*. Late News Poster: QVGA AMOLED Displays Using the Carbon Nanotube Enabled Vertical Organic Light Emitting Transistor. *SID Symposium Digest of Technical Papers* **47**, 1796–1798 (2016).
30. Castro Neto, A. H., Guinea, F., Peres, N. M. R., Novoselov, K. S. & Geim, A. K. The electronic properties of graphene. *Rev. Mod. Phys.* **81**, 109–162 (2009).
31. Geim, A. K. & Novoselov, K. S. The rise of graphene. *Nat. Mater.* **6**, 183–191 (2007).
32. Ando, T. The electronic properties of graphene and carbon nanotubes. *NPG Asia Materials* **1**, 17–21 (2009).
33. Han, T.-H. *et al*. Extremely efficient flexible organic light-emitting diodes with modified graphene anode. *Nat. Photon.* **6**, 105–110 (2012).
34. Li, N. *et al*. Efficient and bright organic light-emitting diodes on single-layer graphene electrodes. *Nat. Commun.* **4**, 2294 (2013).
35. Park, B., Huh, J. N., Lee, W. S. & Bae, I.-G. Simple and rapid cleaning of graphenes with a 'bubble-free' electrochemical treatment. *J. Mater. Chem. C* **6**, 2234–2244 (2018).
36. Köhler, A. & Bässler, H. *Electronic Processes in Organic Semiconductors: An Introduction*. (Wiley-VCH, Verlag GmbH & Co. KGaA, 2015).
37. Fowler, R. H. & Nordheim, L. Electron Emission in Intense Electric Fields. *Proc. R. Soc. Lond. Ser. A* **119**, 173–181 (1928).
38. Sze, S. M. *Physics of Semiconductor Devices*. (Wiley, New York, 1981).
39. Chiguvare, Z., Parisi, J. & Dyakonov, V. Current limiting mechanisms in indium-tin-oxide/poly3-hexylthiophene/aluminum thin film devices. *J. Appl. Phys.* **94**, 2440–2448 (2003).
40. Blum, R., Sprave, M., Sablotny, J. & Eich, M. High-electric-field poling of nonlinear optical polymer. *J. Opt. Soc. Am. B* **15**, 318–328 (1998).
41. Saker, B. K. & Khondaker, S. I. Thermionic Emission and Tunneling at Carbon Nanotube-Organic Semiconductor Interface. *ACS Nano* **6**, 4993–4999 (2012).
42. Koehler, M. & Hümmelgen, I. A. Temperature dependent tunnelling current at metal/polymer interfaces-potential barrier height determination. *Appl. Phys. Lett.* **70**, 3254–3256 (1997).
43. Roman, L. S., Hümmelgen, I. A., Nart, F. C., Péres, L. O. & de Sá, E. L. Determination of electroaffinity and ionization potential of conjugated polymers via Fowler–Nordheim tunnelling measurements: Theoretical formulation and application to poly(p-phenylene vinylene). *J. Chem. Phys.* **105**, 10614–10620 (1996).
44. Yang, H. *et al*. Graphene Barristor, a Triode Device with a Gate-Controlled Schottky Barrier. *Science* **336**, 1140–1143 (2012).
45. Greczynski, G., Kugler, T. & Salaneck, W. R. Characterization of the PEDOT-PSS system by means of X-ray and ultraviolet photoelectron spectroscopy. *Thin Solid Films* **354**, 129–135 (1999).
46. Li, Y. *et al*. Magnetron Sputtered nc-Al/α-Al_2O_3 Nanocomposite Thin Films for Nonvolatile Memory Application. *J. Nanosci. Nanotechnol.* **9**, 4116–4120 (2009).
47. Bokdam, M., Cakir, D. & Brocks, G. Fermi level pinning by integer charge transfer at electrode-organic semiconductor interfaces. *Appl. Phys. Lett.* **98**, 113303 (2011).
48. Park, B. *et al*. Work function optimization of graphene electrodes by MoO_3 doping for efficient light-emitting transistor devices. *Manuscript in preparation* (2018).
49. Johnson, R. W., Hultqvist, A. & Bent, S. F. A brief review of atomic layer deposition: from fundamentals to applications. *Mater. Today* **17**, 236–246 (2014).
50. Li, X. *et al*. Large-Area Synthesis of High-Quality and Uniform Graphene Films on Copper Foils. *Science* **324**(5932), 1312–1314 (2009).

Acknowledgements

The authors acknowledge the helpful assistance of Ms A. Yushika and Mr. Jaewoo Park. This work was supported by a grant from the National Research Foundation of Korea (NRF) funded by the Korean Government (MEST) (2017R1A2A1A17069729). This research was partially supported by the research support of LG Electronics and LG Display. The present research was also supported by a research grant from Kwangwoon University (2019).

Author Contributions

B.P. conceived and supervised the research, while W.S.L., S.Y.N., J.N.H., and I.G.B. conducted all of the experimental work. All authors discussed the results. B.P. wrote the text of the main manuscript and prepared the figures, with contributions from all authors, and S.Y.N. and I.G.B. helped with the editing.

Additional Information

Supplementary information accompanies this paper at https://doi.org/10.1038/s41598-019-42800-y.

Competing Interests: The authors declare no competing interests.

Publisher's note: Springer Nature remains neutral with regard to jurisdictional claims in published maps and institutional affiliations.